Monthly Notices
of the
ROYAL ASTRONOMICAL SOCIETY

MNRAS **455,** 1375–1384 (2016) doi:10.1093/mnras/stv2393

Update on the GRB universal scaling $E_{\rm X,iso}$–$E_{\gamma,\rm iso}$–$E_{\rm pk}$ with 10 years of *Swift* data

E. Zaninoni,[1⋆] M. G. Bernardini,[2] R. Margutti[3] and L. Amati[4]

[1] *ICRANet-Rio, Centro Brasileiro de Pesquisas Físicas, Rua Dr. Xavier Sigaud 150, 22290-180 Rio de Janeiro, Brazil*
[2] *INAF – Osservatorio Astronomico di Brera, via Bianchi 46, I-23807 Merate, Italy*
[3] *Harvard–Smithsonian Center for Astrophysics, 60 Garden Street, Cambridge, MA 02138, USA*
[4] *INAF, Istituto di Astrofisica Spaziale e Fisica Cosmica, Bologna, Via Gobetti 101, I-40129 Bologna, Italy*

Accepted 2015 October 13. Received 2015 October 13; in original form 2015 June 3

ABSTRACT

From a comprehensive statistical analysis of *Swift* X-ray light curves of gamma-ray bursts (GRBs) collected from 2004 December to the end of 2010, we found a three-parameter correlation between the isotropic energy emitted in the rest-frame 1–10^4 keV energy band during the prompt emission ($E_{\gamma,\rm iso}$), the rest-frame peak of the prompt emission energy spectrum ($E_{\rm pk}$), and the X-ray energy emitted in the rest-frame 0.3–30 keV observed energy band ($E_{\rm X,iso}$), computed excluding the contribution of the flares. In this paper, we update this correlation with the data collected until 2014 June, expanding the sample size with ∼35 per cent more objects, where the number of short GRBs doubled. With this larger sample, we confirm the existence of a universal correlation that connects the prompt and afterglow properties of long and short GRBs. We show that this correlation does not depend on the X-ray light-curve morphology and that further analysis is necessary to firmly exclude possible biases derived by redshift measurements. In addition, we discuss about the behaviour of the peculiar objects as ultra-long GRBs and we propose the existence of an intermediate group between long and short GRBs. Interestingly, two GRBs with uncertain classification fall into this category. Finally, we discuss the physics underlying this correlation, in the contest of the efficiency of conversion of the prompt gamma-ray emission energy into the kinetic energy of the afterglow, the photospheric model, and the cannonball model.

Key words: radiation mechanisms: non-thermal – gamma-rays: general – X-rays: general.

1 INTRODUCTION

The *Swift* satellite (Gehrels et al. 2004), launched in 2004 November, opened a new era for the study and understanding of gamma-ray bursts (GRBs), detecting more than 900 objects until 2015 January. Thanks to its unique observing capabilities, many correlations involving prompt and afterglow emission quantities could be further investigated (e.g. Reichart et al. 2001; Amati et al. 2002; Ghirlanda, Ghisellini & Lazzati 2004; Yonetoku et al. 2004; Dainotti, Cardone & Capozziello 2008).

One of the most studied is the Amati relation (Amati et al. 2002) that involves the isotropic energy emitted in the rest-frame 1–10^4 keV energy band during the prompt emission ($E_{\gamma,\rm iso}$) and the photon energy at which the prompt emission energy spectrum peaks ($E_{\rm pk}$). This relation is followed by long GRBs, while short GRBs lie in a separate region of the $E_{\gamma,\rm iso}$–$E_{\rm pk}$ plane. Recent papers (e.g. Zhang, Chen & Huang 2012; Calderone et al. 2015; Shahmoradi & Nemiroff 2015) showed that short GRBs also follow a well-defined relation in the $E_{\gamma,\rm iso}$–$E_{\rm pk}$ plane, with similar slope but different normalization with respect to long GRBs.

From a comprehensive statistical analysis of *Swift* X-ray light curves collected from 2004 December until 2010 December (Margutti et al. 2013, hereafter M13), we found a three-parameter correlation between $E_{\gamma,\rm iso}$, $E_{\rm pk}$, and the X-ray energy emitted in the rest-frame 0.3–30 keV observed energy band excluding the flare activity ($E_{\rm X,iso}$). The uniqueness of this correlation is that it accommodates long, short, and low-energy GRBs in a single scaling, involving prompt and afterglow emission quantities (Bernardini et al. 2012, hereafter B12; M13). This finding suggests that its physical origin is deeply connected with properties that are shared by the GRBs as a whole.

In this paper, we update the $E_{\rm X,iso}$–$E_{\gamma,\rm iso}$–$E_{\rm pk}$ correlation including all GRBs observed by *Swift* until 2014 June. We select the sample following the same prescriptions as in B12 and M13. In particular, we consider only GRBs with (i) secure redshift measurement, (ii) measured $E_{\rm pk}$, and (iii) complete X-ray light curve. The new sample contains about 35 per cent more GRBs than the old one, and, in

⋆E-mail: elena.zaninoni@gmail.com

Table 1. List of 33 GRBs added to the old sample. Short GRBs are marked in boldface, while the GRB with uncertain classification is underlined.

GRB name
080123, 090426, **100117A**, **100625A**, 110106B, 110205A, 110213A, 110503A, 110715A, 110731A, 110801A, 110818A, 111107A, **111117A**, 111209A, 111228A, 120119A, 120326A, 120712A, 120802A, 120811C, 121128A, 130408A, 130427A, 130505A, **130603B**, 130701A, 130831A, 130907A, 130925A, 131030A, 140206A, 140419A

particular, twice the number of short GRBs. This new sample gives us the possibility to better investigate (i) the role of short GRBs in the $E_{\rm X,iso}$–$E_{\gamma,\rm iso}$–$E_{\rm pk}$ correlation, (ii) the possible link between long and short GRBs, (iii) the properties of the group of GRBs that lies between long and short GRBs (which we call *intermediate group*), (iv) the characteristics of peculiar GRBs, like ultra-long GRBs, and (v) the relation between prompt and afterglow emission.

This paper is organized as follows: description of criteria used for the sample selection (Section 2); description of the $E_{\rm X,iso}$–$E_{\gamma,\rm iso}$–$E_{\rm pk}$ correlation and of particular GRBs included in the sample (i.e. short GRBs, ultra-long GRBs, and GRBs with uncertain classification; Section 3); discussion of intermediate group, possible biases, and the physical motivations for this correlation (Section 4); summary and conclusions (Section 5). Uncertainties are given at the 68 per cent confidence level (c.l.) unless explicitly mentioned. Standard cosmological quantities have been adopted: $H_0 = 70$ km s^{-1} Mpc^{-1},$\Omega_\Lambda = 0.7$, and $\Omega_{\rm M} = 0.3$.

2 SAMPLE SELECTION

We updated our sample (B12; M13) selecting all GRBs observed until 2014 June that fulfil the following requirements (M13).

(i) Their redshifts z are derived from optical spectroscopy or they have photometric redshifts for which potential sources of degeneracy (e.g. dust extinction) can be ruled out with high confidence.

(ii) It was possible to measure the rest-frame peak energy ($E_{\rm pk}$) and prompt emission isotropic energy in the rest-frame 1–10^4 keV energy band ($E_{\gamma,\rm iso}$; Amati 2006; Amati et al. 2008; Amati, Frontera & Guidorzi 2009) from the broad-band modelling of the prompt emission time-integrated spectrum.

(iii) They were observed by *Swift*/XRT and have a complete X-ray light curve, i.e. promptly re-pointed by *Swift*/XRT ($t_{\rm rep} <$ 300 s) and for which observations were not limited by any observing constraint.

We obtained a new sample composed of 81 long GRBs, 11 short GRBs, and 2 GRBs with uncertain classification.[1] The new sample contains ∼35 per cent more GRBs than the previous one, in particular the sample of short GRBs doubled (Table 1).

3 THE $E_{\rm X,iso}$–$E_{\gamma,\rm iso}$–$E_{\rm pk}$ CORRELATION

The $E_{\rm X,iso}$–$E_{\gamma,\rm iso}$–$E_{\rm pk}$ correlation involves $E_{\rm pk}$, $E_{\gamma,\rm iso}$, and $E_{\rm X,iso}$. $E_{\rm pk}$ and $E_{\gamma,\rm iso}$ are calculated as described in Amati et al. (2002), where the gamma-ray spectrum is fitted using a Band function (Band et al. 1993). For the short GRBs 080123, 090423, 100625A, 111117A, and 130603B, we consider the values of $E_{\rm pk}$ and $E_{\gamma,\rm iso}$ reported in D'Avanzo et al. (2014), who fitted the spectrum considering also a cut-off power-law function or a Band function with fixed high-energy index.

For GRBs in the original sample, we extracted the XRT light curves using the method presented in Margutti (2009), while for GRBs observed after 2010 December, we used the count rate light curves from the official repository site (Evans et al. 2007, 2009) and employed the time-resolved spectral analysis to perform the spectral calibration in the common rest-frame energy band 0.3–30 keV. In both cases, we use a time-variable flux-to-count conversion factor and we propagate the uncertainty from the spectral fits to the final flux light curves. This method allows us to correctly detect the presence of statistically significant positive temporal fluctuations superimposed on a smoothly decaying light curve. Finally, $E_{\rm X,iso}$ was calculated as in M13, fitting the continuum part of 0.3–30 keV X-ray light curves in luminosity (Margutti et al. 2011; M13; Zaninoni 2013) and integrating the fitted light curve between the start and the end time of the observations. We compute the $E_{\rm X,iso}$ in the 0.3–30 keV band for considering the bulk of the X-ray emission. On the other hand, as we demonstrate in B12 and M13, the choice of the 0.3–30 rest-frame band or of the 0.3–10 keV observer band does not influence the reliability of the correlation.

In Table A1 in Appendix A, we listed the values of $E_{\rm X,iso}$, $E_{\gamma,\rm iso}$, and $E_{\rm pk}$ for the new GRBs of our sample.

The correlation is derived using the method of D'Agostini (2005, for details see Appendix A), which considers an intrinsic scatter $\sigma_{\rm ext}$ that accounts for the possible contribution of hidden variables[2] (see also B12; M13). In this way:

$$\log\left[\frac{E_{\rm X,iso}}{\rm erg}\right] = (0.97\pm0.06)\log\left[\frac{E_{\gamma,\rm iso}}{\rm erg}\right] - (0.57\pm0.13)\log\left[\frac{E_{\rm pk}}{\rm keV}\right] - (0.62\pm0.08), \quad (1)$$

with an extra scatter $\sigma_{\rm ext} = 0.32 \pm 0.04$. Fig. 1 shows a two-dimensional representation of this relation. The extra scatter is similar to the value obtained with the old sample (B12; M13). As explained in B12 and M13, this correlation is robust, spanning four orders of magnitude in $E_{\rm X,iso}$ and $E_{\rm pk}$, and six orders of magnitude in $E_{\gamma,\rm iso}$, and combines both short and long GRBs in a common scaling. Indeed, the newly added short GRBs (080123, 100117A, 100625A, 111117A, 130603B; Table 2) confirm the validity of the $E_{\rm X,iso}$–$E_{\gamma,\rm iso}$–$E_{\rm pk}$ correlation for all families of GRBs and populate the same region of the plane as short GRBs of the original sample.

If we consider only long GRBs, the relation becomes

$$\log\left[\frac{E^{\rm L}_{\rm X,iso}}{\rm erg}\right] = (0.77\pm0.14)\log\left[\frac{E^{\rm L}_{\gamma,\rm iso}}{\rm erg}\right] - (0.21\pm0.24)\log\left[\frac{E^{\rm L}_{\rm pk}}{\rm keV}\right] - (0.63\pm0.08), \quad (2)$$

with an extra scatter $\sigma_{\rm ext} = 0.31 \pm 0.04$. The extra scatter is similar to that of the entire sample, while the slope is slightly different.

We test the $E_{\rm X,iso}$–$E_{\gamma,\rm iso}$–$E_{\rm pk}$ correlation computing the correlation coefficient (ρ_{xy}) and the null hypothesis probability (NHP) for the new and the old sample. In the case of the complete samples, we obtain $\rho^{\rm new}_{xy} = 0.92$ and ${\rm NHP}_{\rm new} \sim 1$ for the updated sample (94 GRBs) and $\rho^{\rm old}_{xy} = 0.90$ and ${\rm NHP}^{\rm old} \sim 1$ for the old sample (61 GRBs); if we consider only long GRBs, we obtain

[1] The GRBs with uncertain classification are GRB 090426 and GRB 100816A. A detailed discussion can be found in Section 3.2.

[2] For this analysis, we use a procedure that uses R (http://www.r-project.org/) program language.

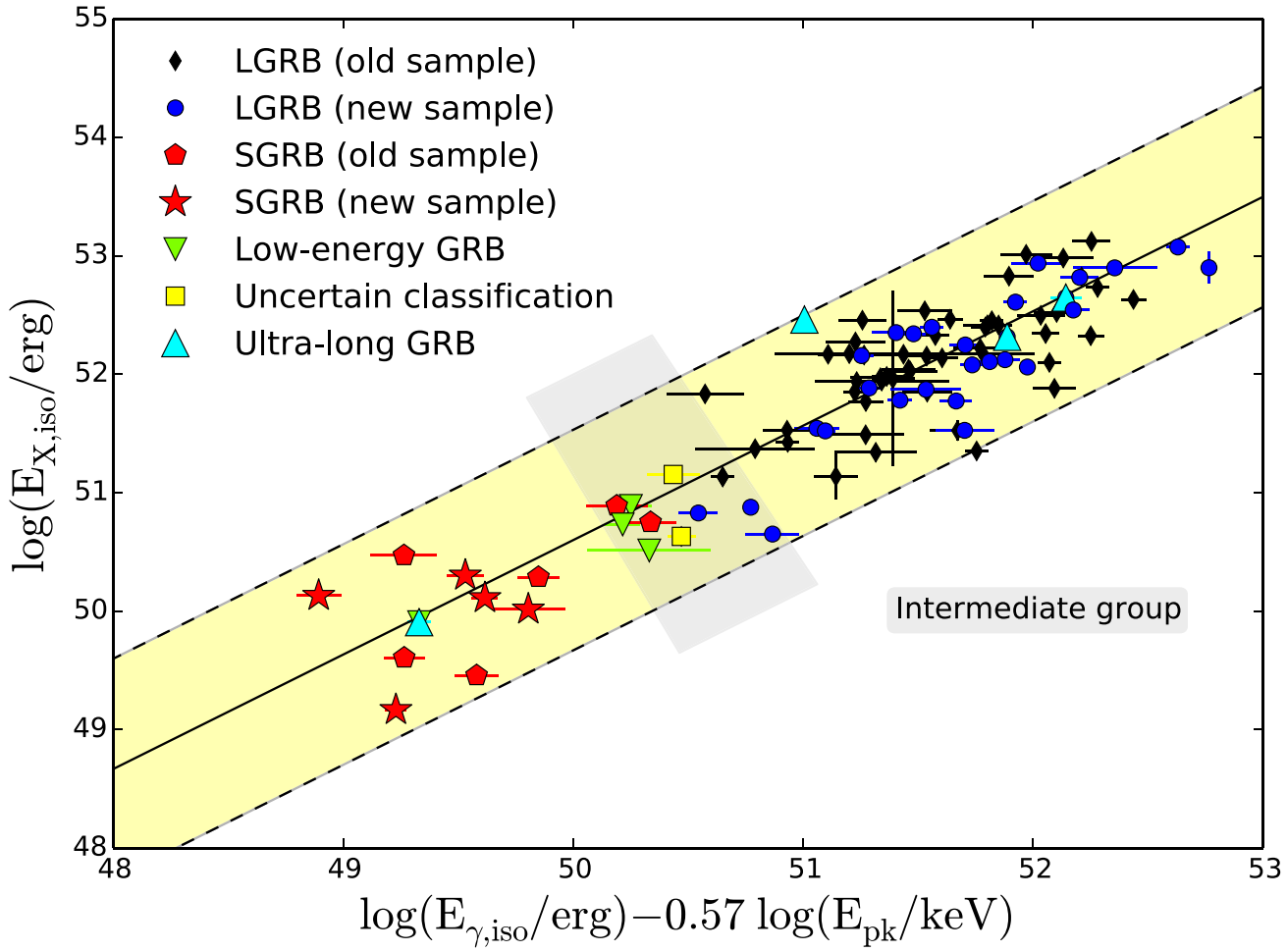

Figure 1. $E_{\rm X,iso}$–$E_{\gamma,\rm iso}$–$E_{\rm pk}$ correlation for the sample of 81 long GRBs (black diamonds for the old sample, blue dots for the new sample, green triangles for low-energy GRBs, and cyan triangles for the ultra-long GRBs), 11 short GRBs (red pentagons for the old sample and red stars for the new sample), and 2 GRBs with uncertain classification (yellow squares). The black solid line is the best-fitting function $\log[E_{\rm x,iso}] = 0.96\ \log[E_{\gamma,\rm iso}] - 0.57\ \log[E_{\rm pk}] - 0.62$ and the yellow area marks the 2σ confidence region. The grey area indicates the position of the intermediate group.

Table 2. Short GRBs. GRB: GRB name. z: redshift. $E_{\rm pk}$: peak energy in keV units. Notes: it indicates if the GRB belongs to the original sample (OS) or to the new sample (NS) and if it was used for the fit of the $E_{\rm X,iso}$–$E_{\gamma,\rm iso}$–$E_{\rm pk}$ correlation (Y) or not (N). z ref. and $E_{\rm pk}$ ref.: reference for the redshift and the $E_{\rm pk}$, respectively. (1) M13; (2) D'Avanzo et al. (2014); (3) Berger et al. (2013); (4) Margutti et al. (2012); (5) Sakamoto et al. (2005); (6). Amati et al. (2008).

GRB	z	$E_{\rm pk}$ (keV)	Notes		z ref.	$E_{\rm pk}$ ref.
050724	0.258	100 ± 16	OS	Y	(1)	(1)
051221A	0.5465	622 ± 35	OS	Y	(1)	(1)
051227	0.714	$100^{+219}_{-41.3}$	NS	N	(1)	(5)
061006	0.438	955 ± 259	OS	Y	(1)	(1)
061201	0.111	969 ± 412	NS	N	(6)	(6)
070714B	0.92	215 ± 750	OS	Y	(1)	(1)
071227	0.3830	1384 ± 277	OS	Y	(1)	(1)
080123	0.495	149.50	NS	Y	(2)	(2)
090510	0.903	8370 ± 760	OS	Y	(1)	(1)
100117A	0.92	551 ± 135	NS	Y	(1)	(1)
100625A	0.452	701.32 ± 114.71	NS	Y	(2)	(2)
101219A	0.718	842 ± 170	NS	N	(2)	(2)
111117A	1.2	966 ± 322	NS	Y	(4)	(2)
120804A	1.3	310	NS	N	(3)	(3)
130603B	0.356	900 ± 140	NS	Y	(2)	(2)

$\rho_{xy}^{\rm new,long} = 0.86$ and $\rm NHP_{new,\,long} \sim 1$ for the updated sample (81 GRBs) and $\rho_{xy}^{\rm old} = 0.84$ and $\rm NHP_{old,long} \sim 1$ for the old sample (54 GRBs). Therefore, the existence of this correlation is confirmed and, since ρ_{xy} and NHP are larger for the updated sample than the old one, we can conclude that the correlation is stronger.

3.1 Ultra-long GRBs

Recently, there has been extensive discussion about the existence of a new class of GRBs, named ultra-long GRBs (e.g. Thöne et al. 2011b; Gendre et al. 2012, 2013; Virgili et al. 2013; Levan et al. 2014; Zhang et al. 2014). From the point of view of the duration of the prompt emission of GRBs, some authors classify as ultra-long GRBs those bursts with durations of several thousand seconds (e.g. Levan et al. 2014), while other authors give a more precise definition: long GRBs have $T_{90} > 2$ s, very long GRBs have $T_{90} > 10^3$ s, while ultra-long GRBs have $T_{90} > 10^4$ s (e.g. Gendre et al. 2013).[3] Only a few very long and ultra-long GRBs were observed so far. Among these, *Swift* detected low-energy GRBs[4] 060218 ($T_{90} = 2100$ s; Cusumano et al. 2006) and 100316D ($T_{90} > 1300$ s; Stamatikos et al. 2010), and GRBs 101225A ($T_{90} \geq 1650$ s; Racusin et al. 2010), 111209A ($T_{90} \sim 15\,000$ s; Hoversten et al. 2011), and 130925A ($T_{90} \sim 20\,000$ s, Lien et al. 2013).

In our sample, there are three ultra-long-lasting bursts: low-energy GRB 060218 and GRBs 111209A and 130925A. In what follows, we also consider GRB 101225A, which was not considered in our previous sample because of the uncertainty of its redshift (Campana et al. 2011; Thöne et al. 2011b), now settled to be 0.847 (Levan et al. 2014). Ultra-long GRBs do not occupy a particular area in the $E_{\gamma,\rm iso}$–$E_{\rm pk}$–$E_{\rm X,iso}$ plane (Fig. 1, cyan triangles). In particular, GRB 060218 is a low-energy GRB and lies consistently in the bottom-left area of this plane, while GRB 111209A and GRB 130925A lie in the region occupied by other long GRBs. GRB 101225A follows the $E_{\rm X,iso}$–$E_{\gamma,\rm iso}$–$E_{\rm pk}$ correlation and behaves as a long GRB. When we consider other two-parameter correlations $E_{\gamma,\rm iso}$–$E_{\rm pk}$ (Fig. 3a), $E_{\rm pk}$–$E_{\rm X,iso}$ (Fig. 3b), $E_{\gamma,\rm iso}$–$E_{\rm X,iso}$ (Fig. 3c), and $E_{\rm pk}$–ϵ ($\epsilon = 1/\eta$, with η the efficiency of the process, see Section 4.3 for more details; Fig. 3d), we notice that GRBs 101225A, 111209A, and 130925A behave like ordinary long GRBs, while GRB 060218 lies in a peculiar area because of its low energies both in the X-rays and gamma-rays.[5]

Ultra-long GRBs are consistent with the $E_{\rm X,iso}$–$E_{\gamma,\rm iso}$–$E_{\rm pk}$ correlation as all other GRBs. Even if these GRBs seem to show uncommon local properties (e.g. Levan et al. 2014), their similar behaviour in the $E_{\rm X,iso}$–$E_{\gamma,\rm iso}$–$E_{\rm pk}$ correlation could be related to a general and not local feature, as the dynamics of the jet.

3.2 GRBs with uncertain classification

GRBs 090426 and 100816A have an uncertain classification, because they show properties that are intermediate between long and short GRBs. From Fig. 1, we note that short GRBs occupy the bottom-left part of the correlation plane, instead GRB 090426 lies between the groups of long and short GRBs. Indeed, the classification of this GRB is much debated (e.g. Antonelli et al. 2009; Levesque et al. 2010; Nicuesa Guelbenzu et al. 2011; Thöne et al. 2011a; Grupe et al. 2013; D'Avanzo et al. 2014). Even if GRB 090624 has a very soft spectral index and it lies in the 2σ c.l. region of the Amati relation, we consider this burst as a short GRB, as discussed also by other authors (e.g. D'Avanzo et al. 2014). Its gamma-ray emission duration is less than 2 s ($T_{90}^{\rm obs} < 0.2$ s and $T_{90}^{\rm RF} < 0.5$ s). In addition, the value of the intrinsic absorption ($N_{\rm H} = 2.3^{+5.6}_{-19} \times 10^{21}$ cm^{-2}), the presence of the highly ionized absorption lines, the position of the afterglow in the host galaxy, and the duration of the gamma-ray emission support the idea that GRB 090426 was formed by the merger of two compact objects. In some scenarios (e.g. Perna & Belczynski 2002; Belczynski et al. 2006), the duration of the merger is very short and the binary system remains inside the star-forming region, as observed in this case, so the afterglow luminosity could be comparable to that of long GRBs. This scenario also supports the high redshift of GRB 090426.

GRB 100816A lies between long and short GRB groups in the $E_{\rm X,iso}$–$E_{\gamma,\rm iso}$–$E_{\rm pk}$ correlation and its classification is still uncertain (Norris, Gehrels & Scargle 2011; Tunnicliffe & Levan 2012; M13; D'Avanzo et al. 2014). It can be classified as short GRB because it has a hard spectrum, it lies offset from its host galaxy, and there is no association with a supernova (SN). On the other hand, in strict analogy with long GRBs, it follows the Amati relation, its gamma-ray duration is longer than 2 s ($T_{90} \sim 2.9$ s), and has a positive spectral lag (Bernardini et al. 2015).

4 DISCUSSION

The new sample of GRBs confirms the existence of the $E_{\rm X,iso}$–$E_{\gamma,\rm iso}$–$E_{\rm pk}$ correlation, with similar best-fitting parameters. In particular, the larger number of short GRBs better constrains this correlation, since there are more bursts with low energies. In addition, this correlation is robust, spanning four orders of magnitude in $E_{\rm X,iso}$ and $E_{\rm pk}$, and six orders of magnitude in $E_{\gamma,\rm iso}$, and combining both short and long GRBs in a common scaling. In the following sections, we discuss the presence of an *intermediate* group of GRBs that lies between long and short GRBs in the $E_{\rm X,iso}$–$E_{\gamma,\rm iso}$–$E_{\rm pk}$ correlation plane (Section 4.1), the possible presence of biases that shape the correlation (Section 4.2), and the possible physical processes and mechanisms that lead to the $E_{\rm X,iso}$–$E_{\gamma,\rm iso}$–$E_{\rm pk}$ correlation (Section 4.3).

4.1 The intermediate group

In the previous compilation of the $E_{\rm X,iso}$–$E_{\gamma,\rm iso}$–$E_{\rm pk}$ correlation, GRBs were divided into two groups along the correlation with a lack of objects between them. Thanks to the updated sample, this area is now occupied by three new long GRBs (110106B, 120724A, 130831A) and a GRB with uncertain classification (090426). This group of objects, together with short GRBs 070714B and 090510, low-energy GRBs 050416A, 060614, and 081007, long GRB 080916, and GRB 100816A with uncertain classification, suggest the presence of an intermediate group between long and short GRBs (Fig. 1, grey area).

In this group, there are not only the two GRBs with uncertain classification, which we discussed in Section 3.2, but also another intriguing object, GRB 060614. This GRB has been classified as long GRB because of the duration of its gamma-ray emission ($T_{90} = 102$ s), but it has some characteristics that are typical of short GRBs (e.g. Della Valle et al. 2006; Fynbo et al. 2006; Gal-Yam et al. 2006; Gehrels et al. 2006). In spite of its low redshift

[3] T_{90} is the time in which from 5–95 per cent cumulative counts are recorded.
[4] We consider as low-energy GRBs long GRBs with $E_{\gamma,\rm iso}$ below 10^{52} erg.
[5] GRB 101225A does not lie in the 2σ region for $E_{\rm pk}$–ϵ relation. The uncertainties about the analysis of the data of this GRB prevent us from deriving firm conclusions about its behaviour.

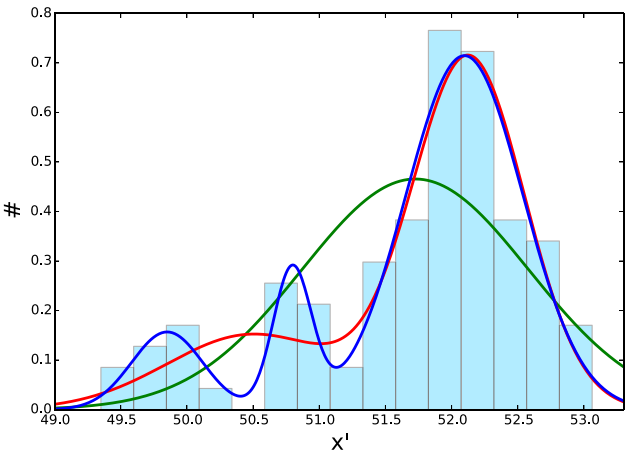

Figure 2. Distribution of GRBs in our sample as projected over the best-fitting function of the $E_{\rm X,iso}$–$E_{\gamma,\rm iso}$–$E_{\rm pk}$ correlation, with x' the coordinate representing the position of the object over this function. We fit the distribution with a Gaussian function (green solid line), the sum of two Gaussian functions (red solid line), and the sum of three Gaussian functions (blue solid line).

($z = 0.125$), no SN has been detected and its environment is typical of short GRBs, since it exploded in a zone with a small specific star formation rate and offset from the GRB host nucleus. On the other hand, its X-ray, UV, and optical light curves and spectral energy distributions are well explained within the standard afterglow model (Mangano et al. 2007; Xue et al. 2009), and it follows the Amati relation as a normal long burst (Amati et al. 2007). Because of the peculiarity of this object, alternative progenitors have been proposed, as a compact binary merger or a massive collapsar that powers a GRB with no association with an SN (e.g. Della Valle et al. 2006; Fynbo et al. 2006; Gal-Yam et al. 2006; Gehrels et al. 2006; Zhang et al. 2007; Caito et al. 2009).

The *Swift*-BAT light curve of the short GRB 070714B shows a short-duration peak followed by a softer, long-lasting tail, called extended emission (EE). One quarter of the detected short GRBs have an EE (Norris, Gehrels & Scargle 2010). Their gamma-ray light curves are similar and uniform and their X-ray light curves have similar plateau luminosities and time-scales (Gompertz et al. 2013). This suggests that they have a common progenitor, which is different from the standard merger scenario for short GRBs, since it must require an injection of energy after the first spike, which switches off around 100 s after the trigger in the rest frame. Several models have been proposed to explain the origin of these objects; for example, the central engine for these bursts could be a magnetar (e.g. Metzger, Quataert & Thompson 2008; Bucciantini et al. 2012; Gompertz et al. 2013).

Fig. 2 shows the distribution of GRBs in our sample as projected over the best-fitting function of the $E_{\rm X,iso}$–$E_{\gamma,\rm iso}$–$E_{\rm pk}$ correlation, with x' the coordinate representing the position of the data points over this new reference axis (e.g. the best-fitting function).[6] Following the procedure used by Horváth et al. (2008), we fit the distribution with a single Gaussian function ($G1$), with the sum of two Gaussian functions ($G2$), and then with the sum of three Gaussian functions ($G3$) using the maximum likelihood method.[7] The maximum values of the log-likelihood functions are, respectively, -120.12, -104.58 and -100.41. We perform a likelihood ratio (LR) test[8] to verify which model fits better this distribution and we obtain $\rm LR_{\mathit{G1},\mathit{G2}} = 31.08$ with p-value $= 0.01$ (DOF $= 3$), $\rm LR_{\mathit{G2},\mathit{G3}} = 8.34$ with p-value $= 0.04$ (DOF $= 3$), and $\rm LR_{\mathit{G1},\mathit{G3}} = 40$ with p-value $= 0$ (DOF $= 6$). From this statistical analysis, we can affirm that the best fit is done with model $G3$.

In the Amati relation (Fig. 3a, Table 3), the intermediate group lies in the low peak energy part of the plane, with the exception of two short GRBs, since the Amati relation is followed only by long GRBs. GRB 090426 and GRB 100816A are within the limit of 2σ of the Amati relation, so they behave as long GRBs (D'Avanzo et al. 2014).

In the $E_{\rm pk}$–$E_{\rm X,iso}$ relation for long GRBs (Fig. 3b, Table 3), GRBs of the intermediate group lie within 2σ from the best-fitting function, with exception of GRB 100816A which falls into 3σ, and short GRBs do not follow this relation.

The $E_{\gamma,\rm iso}$–$E_{\rm X,iso}$ relation is followed by all GRBs of the intermediate group (Fig. 3c, cyan and grey areas, respectively; Table 3).

The region of the $E_{\rm X,iso}$–$E_{\gamma,\rm iso}$–$E_{\rm pk}$ correlation plane occupied by this group could be considered as an intermediate zone. In this area, we find both low- and high-energy GRBs. These objects have similar X-ray energies around 10^{51} erg, but very different peak energies. The isotropic X-ray energy of both short and long GRBs linearly increases with the isotropic gamma-ray energy with the same scaling law (Fig. 3c), while, for a given isotropic gamma-ray energy or a fixed X-ray energy, short GRBs have higher peak energies than long GRBs (Figs 3a and b).

In addition, the majority of GRBs in the intermediate group have a redshift <1, except for short GRB 090426 ($z = 2.609$) and GRB 120724A ($z = 1.48$), and long GRBs belonging to this group have typical durations ($T_{90} \leq 80$ s, GRB 070714B). Their X-ray light curves have a canonical shape, with an initial steep decay, followed by a plateau of small duration and/or steeper than usual and a normal decay phase.[9]

Indeed, these GRBs have small redshifts, like short GRBs, and are less energetic than long one, even if they have typical long GRB durations. They have canonical X-ray light curves and they show limited flaring activity. Therefore, they seem to represent a transitional group between GRBs with low energies and simple X-ray light curves (e.g. single or double power laws or canonical shapes) and more energetic long GRBs, with also complex and unusual X-ray light curves (e.g. with a shallow phase before the steep decay or with big flares). A larger sample is needed to confirm or rule out the presence of an intermediate group.

[6] If, e.g., $P(x_{\rm P}; y_{\rm P})$ is the data point and $y = mx + q$ is our best-fitting function, the coordinate x' is the x-coordinate of the intersection point between the line that passes for the point P and perpendicular to the best-fitting function, and the best-fitting function itself. In this way, $x' = (m/(m^2+1))(y_{\rm P} - q + (x_{\rm P}/m))$.

[7] For this analysis, we minimize the negative logarithm of the likelihood function using the procedure `scipy.optimize.minimize` of PYTHON program language (https://www.python.org/). For the three fit functions considered, we obtain (a) single Gaussian function: $\mu = 51.73$ and $\sigma = 0.86$; (b) sum of two Gaussian functions: $\mu_1 = 50.50$, $\sigma_1 = 0.65$, $\mu_2 = 52.13$, and $\sigma_2 = 0.42$; (c) sum of three Gaussian functions: $\mu_1 = 49.85$, $\sigma_1 = 0.27$, $\mu_2 = 50.80$, $\sigma_2 = 0.14$, $\mu_3 = 52.10$, and $\sigma_3 = 0.44$.

[8] We define LR $= 2$ [ln(L1) $-$ ln(L2)], with L1 and L2 the maximum log-likelihood for the simpler model and the more complicated model, respectively. Since LR $\sim \chi^2$, with the degrees of freedom (DOF) equal to the number of additional parameters in the more complex model, we can calculate the p-value. If p-value < 0.05, the more complex model is favourable.

[9] The X-ray light curves of GRBs 050416A and 100816A show a small steep decay, difficult to fit with a canonical shape, while the observations of GRB 120724A stop before 24 000 s after the trigger, suggesting that the normal decay phase might have been missing.

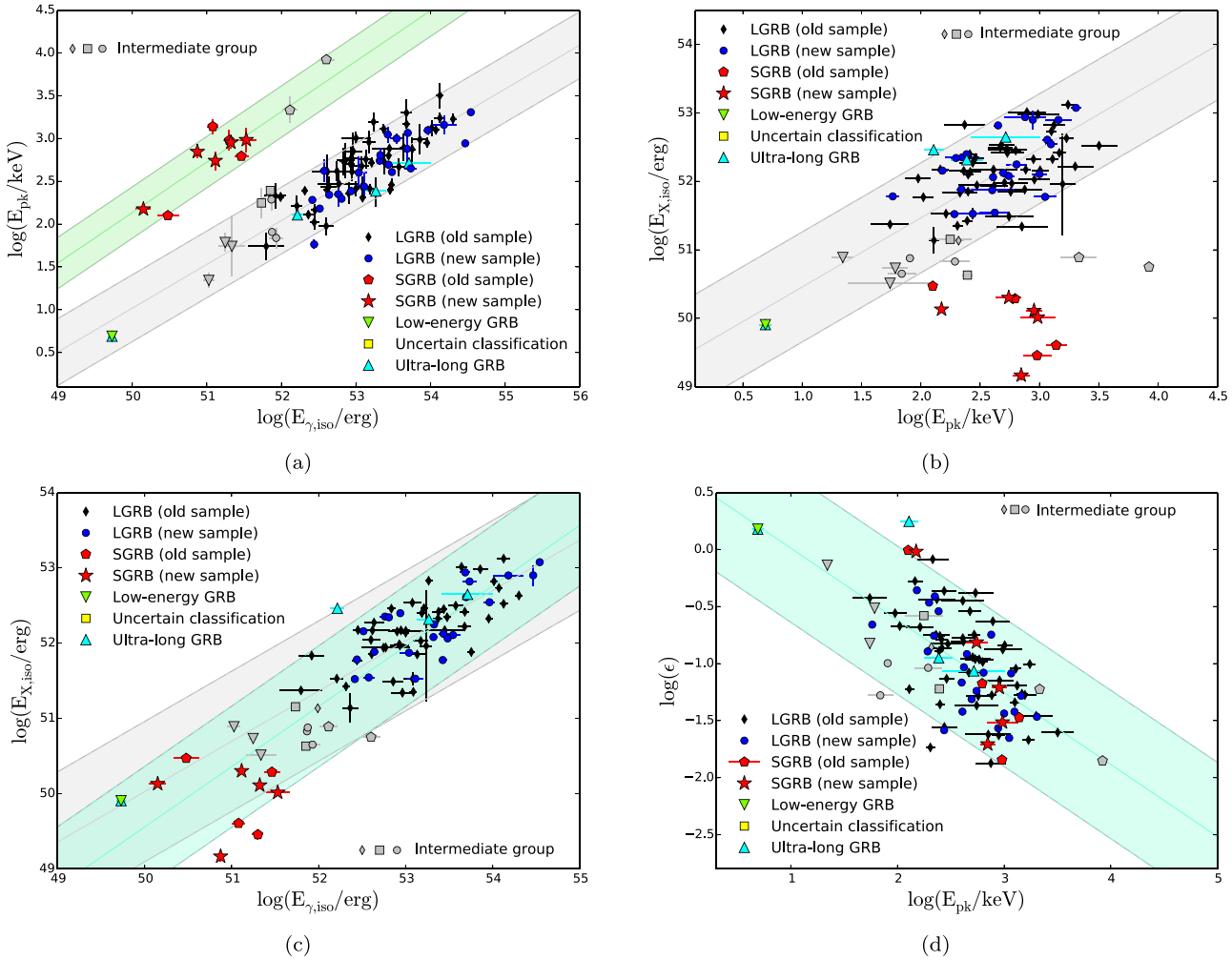

Figure 3. Two-parameter relations. Colour code as Fig. 1. Grey symbols indicate the intermediate group. The grey area indicates that the best fit is computed using only long GRBs, while the cyan area indicates that the best fit is computed using all GRBs of the sample. (a) The Amati relation ($E_{\gamma,\rm iso}$–$E_{\rm pk}$ relation): the green solid line is the best-fitting function for short GRBs as calculated by Calderone et al. (2015) and the green area marks the 2σ region. (b) $E_{\rm x,iso}$–$E_{\rm pk}$ relation. (c) $E_{\gamma,\rm iso}$–$E_{\rm x,iso}$ relation. (d) $E_{\rm pk}$ versus ϵ.

Table 3. From left to right: X and Y parameters to be correlated [the best-fitting law reads $\log(Y) = q + m\log(X)$]; best-fitting parameters as obtained accounting for the sample variance (D'Agostini 2005): slope (m), normalization (q), intrinsic scatter (σ); errors are given at the 95 per cent c.l. For each parameter couple, values reported in the first line refer to the entire sample, while in the second line we restrict our analysis to the long GRB class. $E_{\rm X,iso}$ and $E_{\gamma,\rm iso}$ are normalized to 10^{52} erg, while $E_{\rm pk}$ to 100 keV.

X	Y	m	q	σ
$E_{\gamma,\rm iso}$	$E_{\rm X,iso}$	0.80 ± 0.06	-0.84 ± 0.08	0.40 ± 0.04
		0.68 ± 0.06	-0.64 ± 0.08	0.32 ± 0.04
$E_{\gamma,\rm iso}$	$E_{\rm pk}$	0.26 ± 0.03	0.38 ± 0.07	0.38 ± 0.04
		0.51 ± 0.04	0.04 ± 0.05	0.19 ± 0.02
$E_{\rm pk}$	$E_{\rm X,iso}$	0.57 ± 0.25	-0.55 ± 0.19	0.83 ± 0.08
		1.01 ± 0.14	-0.53 ± 0.10	0.40 ± 0.05
$E_{\rm pk}$	η	-0.63 ± 0.10	-0.62 ± 0.08	0.32 ± 0.04
		-0.57 ± 0.11	-0.65 ± 0.08	0.31 ± 0.04

4.2 Possible biases

In B12 and M13, we discussed the possible caveat on the definition of $E_{\rm X,iso}$. In particular, we analysed the differences between the values computed in the observer-frame 0.3–10 keV and in the rest-frame 0.3–30 keV, and the arbitrariness of the choice of the interval time for the integration. We concluded that these factors do not influence the $E_{\rm X,iso}$–$E_{\gamma,\rm iso}$–$E_{\rm pk}$ correlation. The $E_{\rm X,iso}$ does not include the contribution of flares, which are present in ~ 40 per cent of light curves of our sample. As we discussed in B12 and M13, the inclusion of flares in the computation of the $E_{\rm X,iso}$ does not influence the $E_{\rm X,iso}$–$E_{\gamma,\rm iso}$–$E_{\rm pk}$ correlation because the energy content

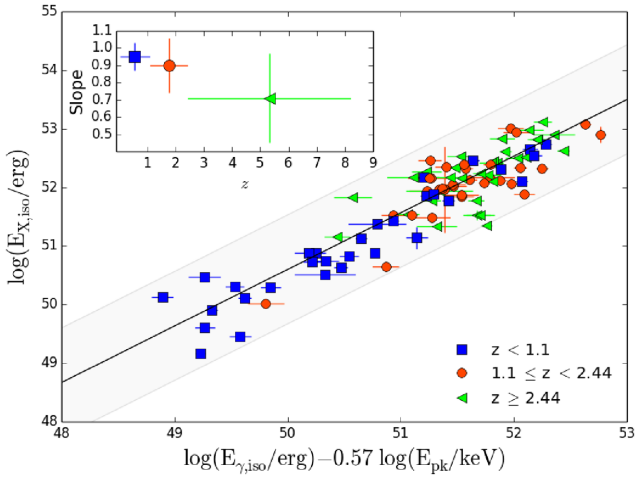

Figure 4. $E_{\rm X,iso}$–$E_{\gamma,\rm iso}$–$E_{\rm pk}$ correlation, considering the differences in redshift for GRBs in our sample. Blue squares: $z < 1.1$; orange dots: $1.1 \leq z < 2.44$; green triangles: $z \geq 2.44$. The black solid line is the best fit function of the complete sample and the grey area marks the 2σ regions. Inset: slopes of the best-fitting function for the three groups.

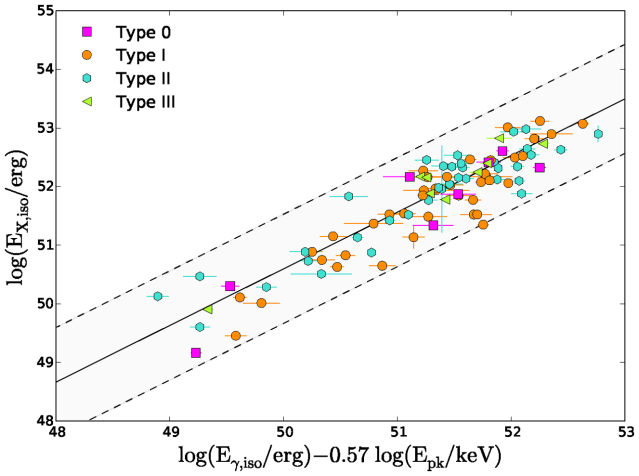

Figure 5. $E_{\rm X,iso}$–$E_{\gamma,\rm iso}$–$E_{\rm pk}$ correlation, considering the different type of X-ray light curves. Pink squares: Type 0; orange dots: Type I; cyan hexagons: Type II; green triangles: Type III. The black solid line is the best-fitting function, as in Fig. 1, and the grey area marks the 2σ regions.

of flares is usually ~ 25 per cent of the underlying continuum $E_{\rm X,iso}$ and the correlation scatter does not better, since the most scattered population in this correlation are short GRBs that have no bright flares (Margutti et al. 2011).

In this section, we examine if the $E_{\rm X,iso}$–$E_{\gamma,\rm iso}$–$E_{\rm pk}$ correlation could be affected by the redshift and by the properties of the X-ray light curve.

Regarding the relation between $E_{\rm X,iso}$ and redshift, in fig. 4 of M13 we showed that we are not sensitive to the population of bursts with $E_{\rm X,iso} < 10^{51}$ erg for $z > 2$; in this way, the low-energy tail of the $E_{\rm X,iso}$ distribution is currently undersampled. This is likely a non-detectability zone. For $z > 1$, there is no evidence for an evolution of the upper bound of $E_{\rm X,iso}$ with redshift, which may suggest that $\sim 10^{53}$ erg is a physical boundary to the $E_{\rm X,iso}$ distribution. M13 underlined that maximum budget $E_{\rm max} \sim 10^{52}$ erg is predicted by magnetar models (Usov 1992).

In Fig. 4, we show the distribution of GRBs in the $E_{\gamma,\rm iso}$–$E_{\rm pk}$–$E_{\rm X,iso}$ plane depending on their redshift z. Low X-ray energy GRBs (short GRBs and low-energy long GRBs) are observed only at low redshift, while long GRBs are observed at every redshift. We divided our sample into three groups with the same number of objects depending on their redshift ($z < 1.1$, 31 GRBs; $1.1 \leq z < 2.44$, 32 GRBs; $z \geq 2.44$, 32 GRBs), and we calculated the best-fitting function for each group;[10] as shown in Fig. 4 (inset), the slope of the correlation does not evolve with z. The error of the slope parameter increases with the z, maybe because of the lack of high-z objects in the bottom-left part of the plane (i.e. low-energy GRBs).[11]

Moreover, the estimation of $E_{\rm X,iso}$, $E_{\gamma,\rm iso}$, and $E_{\rm pk}$ can be influenced by different factors, for example the systematics introduced by the limited energy band of the detector (e.g. Lloyd, Petrosian & Mallozzi 2000; Lloyd-Ronning & Petrosian 2002), the extrapolation made for computing the energies in a rest-frame energy band (e.g. Kocevski & Petrosian 2013), and the choice of the cosmological parameters to calculate the luminosity distance (Amati 2006). On the other hand, since the slope of this correlation is ~ 1, the dependence on the luminosity distance is small.

In particular, analysing $E_{\gamma,\rm iso}$ versus z, we note that there are few very bright GRBs at low redshift: this could be caused by evolutionary effects (i.e. older GRBs are brighter), by a correlation between GRB brightness and jet opening angle (e.g. Ghirlanda et al. 2013), or by a combination of jet structure and viewing angle (e.g. Lazzati et al. 2013). For $E_{\rm pk}$, it is necessary to underline that the maximum detectable $E_{\rm pk}$ depends on the combination between the brightness of the GRBs and the effective collecting area of the instrument with respect to the energy band. Because of these effects, the correlation could be slightly influenced by z, but current data do not allow us to confirm this issue (see for example Fig. 4, inset).

We consider the possibility that the $E_{\rm X,iso}$–$E_{\gamma,\rm iso}$–$E_{\rm pk}$ correlation could be influenced by the different morphology of the X-ray light curve. We classify the X-ray light curves based on the number of break times in their fitting function (M13): *Type 0* is fitted with a single power law, *Type I* with the sum of two power laws, *Type II* (or *canonical*) with the sum of three power laws, and *Type III* with the sum of four power laws. Fig. 5 shows the distribution of GRBs in $E_{\gamma,\rm iso}$–E_{pk}–$E_{\rm X,iso}$ plane depending on their X-ray light-curve morphology. Since GRBs with different X-ray light-curve shapes are equally distributed on the plane, we conclude that the distribution of GRBs in the $E_{\rm X,iso}$–$E_{\gamma,\rm iso}$–$E_{\rm pk}$ plane is not dependent on this feature. In addition, we make the fit considering only the subgroup of canonical X-ray light curves (33 GRBs), and we obtain fit parameters that are consistent with the values computed for the entire sample.[12] Therefore, this correlation is not influenced by the different shapes of the X-ray light curves.

[10] Best-fitting function for the three groups of GRBs: (a) $z < 1.1$, $\log[E_{\rm X,iso}] = (0.95 \pm 0.08)\log[E_{\gamma,\rm iso}] - (0.61 \pm 0.14)\log[E_{\rm pk}] - (0.66 \pm 0.10)$, with $\sigma_{\rm ext} = 0.29 \pm 0.06$; (b) $1.1 \leq z < 2.44$, $\log[E_{\rm X,iso}] = (0.90 \pm 0.16)\log[E_{\gamma,\rm iso}] - (0.47 \pm 0.31)\log[E_{\rm pk}] - (0.61 \pm 0.19)$, with $\sigma_{\rm ext} = 0.32 \pm 0.06$; (c) $z \geq 2.44$, $\log[E_{\rm X,iso}] = (0.71 \pm 0.26)\log[E_{\gamma,\rm iso}] - (0.24 \pm 0.46)\log[E_{\rm pk}] - (0.49 \pm 0.21)$, with $\sigma_{\rm ext} = 0.35 \pm 0.07$.

[11] To prove that the $E_{\gamma,\rm iso}$–$E_{\rm pk}$–$E_{\rm X,iso}$ relation does not depend on z, a further analysis is needed, for example as in Dainotti et al. (2013) for the $L_{\rm X}$–$T_a^\star$ relation, but it is beyond the aim of this paper.

[12] For the subgroup of the canonical X-ray light curves, we calculate $\log[E_{\rm X,iso}] = (0.87 \pm 0.12)\log[E_{\gamma,\rm iso}] - (0.34 \pm 0.24)\log[E_{\rm pk}] - 0.62 \pm 0.13$, if we fix $m_2 = -0.59$ with $\sigma = 0.28 \pm 0.05$.

4.3 Physics and models

As in B12 and M13, we defined $\epsilon = E_{\rm X,iso}/E_{\gamma,\rm iso}$. ϵ represents the opposite of the efficiency, that is the ratio of the prompt emission energy to the outflow kinetic energy (e.g. Lloyd-Ronning & Zhang 2004). As we showed in our previous works (B12; M13), we can divide the plane into two parts: one of the low-energy GRBs which are less efficient and occupy the top-left part of the plane, and the other group composed of short and long GRBs, which have similar efficiencies. For this reason, from this plot it would be impossible to discriminate if GRB 090426A and GRB 100816A are long or short GRBs (grey squares in Fig. 3d).

The physics behind the prompt emission is still one of the main open issues in the study of GRBs, with several emission mechanisms and scenario being proposed. Among these, the photospheric models (e.g. Mészáros & Rees 2000) and the cannonball (CB) model (e.g. Dar & de Rújula 2004) are the ones providing most naturally a physical ground to the $E_{\rm X,iso}$–$E_{\gamma,\rm iso}$–$E_{\rm pk}$ correlation.

The photospheric model considers how the GRB spectrum in the optically thick phase can be modified by the interaction of the radiation field with the leptonic component of the outflow, before it is released at the photosphere (Mészáros & Rees 2000; Rees & Mészáros 2005; Giannios 2006; Lazzati, Morsony & Begelman 2009). The simulations made by Lazzati et al. (2013) can reproduce the $E_{\rm X,iso}$–$E_{\gamma,\rm iso}$–$E_{\rm pk}$ correlation since the radiative efficiency of brighter bursts is higher than that of weaker bursts. However, for adequately comparing observations and simulations, it is necessary to assume a value for the electron equipartition parameter ϵ (Lazzati et al. 2013). They show that, by adopting the fiducial value $\epsilon = 0.1$, good agreement between simulation results and observed values is obtained.

In the CB model (Dar & de Rújula 2004; Dado, Dar & De Rújula 2009a,b), the inverse Compton scattering caused by the interaction between the electrons of the CB plasma and the light in the near ambient of the SN is responsible for the gamma-ray prompt emission of the GRBs, while the afterglow emission is related to the synchrotron radiation of the electrons swept in and accelerated in the CBs. In this model, the $E_{\rm X,iso}$–$E_{\gamma,\rm iso}$–$E_{\rm pk}$ correlation is simply the combination of the two-parameter correlations of kinetic origin that are followed by both long and short GRBs, even if with different normalizations, and so it depends on the large Doppler boosting and the relativistic beaming that strongly influenced the observed radiation (Dado & Dar 2013).

5 SUMMARY AND CONCLUSIONS

In this paper, we confirm the existence of the $E_{\rm X,iso}$–$E_{\gamma,\rm iso}$–$E_{\rm pk}$ correlation by employing a large sample of 94 GRBs (35 per cent more than the previous sample and a double number of short GRBs; B12; M13). The main feature of this correlation is that it involves both prompt and afterglow quantities ($E_{\rm X,iso}$, $E_{\gamma,\rm iso}$, and $E_{\rm pk}$) and it is followed by all kinds of GRBs, both short and long GRBs.

As underlined in previous papers (B12; M13), this correlation implies the existence of common properties between long, short, and low-energy GRBs, even if they have different progenitors and environments.

In particular, in this paper we have shown the following.

(i) The $E_{\rm X,iso}$–$E_{\gamma,\rm iso}$–$E_{\rm pk}$ correlation is followed by ultra-long GRBs (060218, 101225A, 111209A, and 130925A), which do not occupy a particular region in the plane. Indeed, GRBs 101225A, 111209A, and 130925A behave as common long GRBs.

(ii) There is a possible intermediate group of transition between long and short GRBs, composed of different kinds of GRBs. In particular, in this group we find GRBs 090426, 100816A, and 060614 which have uncertain classification since they have properties of both long and short GRBs, and GRB 070714B that is a short GRB with EE.

(iii) We considered the possibility that the correlation could be biased by some assumption or evolve with some parameter. In B12 and M13, we excluded that the $E_{\rm X,iso}$–$E_{\gamma,\rm iso}$–$E_{\rm pk}$ correlation is influenced by the definition of $E_{\rm X,iso}$. Here, we showed that this relation is independent from the X-ray light-curve morphology, indicating its robustness. A deeper analysis is needed to confirm its independence from the redshift.

(iv) As discussed in B12, the $E_{\rm X,iso}$–$E_{\gamma,\rm iso}$–$E_{\rm pk}$ correlation can be expressed in the form of a two-parameter correlation between the GRB efficiency and $E_{\rm pk}$, as shown in Fig. 3(d). The physical origin of such a relation may be connected with the outflow Lorentz factor.

(v) The photospheric model (Lazzati et al. 2013) and the CB model (Dado & Dar 2013) can reproduce this correlation.

This updated sample confirms the existence of the $E_{\rm X,iso}$–$E_{\gamma,\rm iso}$–$E_{\rm pk}$ correlation. More data are necessary to confirm the possible existence of the intermediate group and to understand the possible physical processes that lead $E_{\rm X,iso}$, $E_{\gamma,\rm iso}$, and $E_{\rm pk}$ to be linked.

ACKNOWLEDGEMENTS

We thank the anonymous referee for the helpful comments that have improved this paper. This work made use of data supplied by the UK Swift Science Data Centre at the University of Leicester. EZ thanks Luca Izzo and Marco Muccino for sharing their data. EZ acknowledges the support by the International Cooperation Program CAPES-ICRANet financed by CAPES – Brazilian Federal Agency for Support and Evaluation of Graduate Education within the Ministry of Education of Brazil. MGB thanks support from the T-REX program.

REFERENCES

Amati L., 2006, MNRAS, 372, 233
Amati L. et al., 2002, A&A, 390, 81
Amati L., Della Valle M., Frontera F., Malesani D., Guidorzi C., Montanari E., Pian E., 2007, A&A, 463, 913
Amati L., Guidorzi C., Frontera F., Della Valle M., Finelli F., Landi R., Montanari E., 2008, MNRAS, 391, 577
Amati L., Frontera F., Guidorzi C., 2009, A&A, 508, 173
Antonelli L. A. et al., 2009, A&A, 507, L45
Band D. et al., 1993, ApJ, 413, 281
Belczynski K., Perna R., Bulik T., Kalogera V., Ivanova N., Lamb D. Q., 2006, ApJ, 648, 1110
Berger E. et al., 2013, ApJ, 765, 121
Bernardini M. G., Margutti R., Zaninoni E., Chincarini G., 2012, MNRAS, 425, 1199 (B12)
Bernardini M. G. et al., 2015, MNRAS, 446, 1129
Bucciantini N., Metzger B. D., Thompson T. A., Quataert E., 2012, MNRAS, 419, 1537
Caito L., Bernardini M. G., Bianco C. L., Dainotti M. G., Guida R., Ruffini R., 2009, A&A, 498, 501
Calderone G. et al., 2015, MNRAS, 448, 403
Campana S. et al., 2011, Nature, 480, 69
Cusumano G., Barthelmy S., Gehrels N., Hunsberger S., Immler S., Marshall F., Palmer D., Sakamoto T., 2006, GRB Coordinates Network, 4775, 1
D'Agostini G., 2005, preprint (arXiv:physics/0511182)

D'Avanzo P. et al., 2014, MNRAS, 442, 2342
Dado S., Dar A., 2013, ApJ, 775, 16
Dado S., Dar A., De Rújula A., 2009a, ApJ, 693, 311
Dado S., Dar A., De Rújula A., 2009b, ApJ, 696, 994
Dainotti M. G., Cardone V. F., Capozziello S., 2008, MNRAS, 391, L79
Dainotti M. G., Petrosian V., Singal J., Ostrowski M., 2013, ApJ, 774, 157
Dar A., de Rújula A., 2004, Phys. Rep., 405, 203
Della Valle M. et al., 2006, Nature, 444, 1050
Evans P. A. et al., 2007, A&A, 469, 379
Evans P. A. et al., 2009, MNRAS, 397, 1177
Fynbo J. P. U. et al., 2006, Nature, 444, 1047
Gal-Yam A. et al., 2006, Nature, 444, 1053
Gehrels N. et al., 2004, ApJ, 611, 1005
Gehrels N. et al., 2006, Nature, 444, 1044
Gendre B. et al., 2012, ApJ, 748, 59
Gendre B. et al., 2013, ApJ, 766, 30
Ghirlanda G., Ghisellini G., Lazzati D., 2004, ApJ, 616, 331
Ghirlanda G. et al., 2013, MNRAS, 428, 1410
Giannios D., 2006, A&A, 457, 763
Gompertz B. P., O'Brien P. T., Wynn G. A., Rowlinson A., 2013, MNRAS, 431, 1745
Grupe D., Nousek J. A., Veres P., Zhang B.-B., Gehrels N., 2013, ApJS, 209, 20
Horváth I., Balázs L. G., Bagoly Z., Veres P., 2008, A&A, 489, L1
Hoversten E. A. et al., 2011, GRB Coordinates Network, 12632, 1
Kocevski D., Petrosian V., 2013, ApJ, 765, 116
Lazzati D., Morsony B. J., Begelman M. C., 2009, ApJ, 700, L47
Lazzati D., Morsony B. J., Margutti R., Begelman M. C., 2013, ApJ, 765, 103
Levan A. J. et al., 2014, ApJ, 781, 13
Levesque E. M. et al., 2010, MNRAS, 401, 963
Lien A. Y., Markwardt C. B., Page K. L., Palmer D. M., Racusin J. L., Siegel M. H., Ukwatta T. N., 2013, GRB Coordinates Network, 15246, 1
Lloyd N. M., Petrosian V., Mallozzi R. S., 2000, ApJ, 534, 227
Lloyd-Ronning N. M., Petrosian V., 2002, ApJ, 565, 182
Lloyd-Ronning N. M., Zhang B., 2004, ApJ, 613, 477
Mangano V. et al., 2007, A&A, 470, 105
Margutti R., 2009, PhD thesis, Università degli Studi di Milano-Bicocca, available at: http://hdl.handle.net/10281/7465
Margutti R. et al., 2011, MNRAS, 417, 2144
Margutti R. et al., 2012, ApJ, 756, 63
Margutti R. et al., 2013, MNRAS, 428, 729 (M13)
Mészáros P., Rees M. J., 2000, ApJ, 530, 292
Metzger B. D., Quataert E., Thompson T. A., 2008, MNRAS, 385, 1455
Nicuesa Guelbenzu A. et al., 2011, A&A, 531, L6
Norris J. P., Gehrels N., Scargle J. D., 2010, ApJ, 717, 411
Norris J. P., Gehrels N., Scargle J. D., 2011, ApJ, 735, 23
Perna R., Belczynski K., 2002, ApJ, 570, 252
Racusin J. L. et al., 2010, GRB Coordinates Network, 11493, 1
Rees M. J., Mészáros P., 2005, ApJ, 628, 847
Reichart D. E., Lamb D. Q., Fenimore E. E., Ramirez-Ruiz E., Cline T. L., Hurley K., 2001, ApJ, 552, 57
Sakamoto T. et al., 2005, GRB Coordinates Network, 4403, 1
Shahmoradi A., Nemiroff R. J., 2015, MNRAS, 451, 126
Stamatikos M., Barthelmy S. D., Baumgartner W. H., Beardmore A. P., Campana S., 2010, GRB Coordinates Network, 10496, 1
Thöne C. C. et al., 2011a, MNRAS, 414, 479
Thöne C. C. et al., 2011b, Nature, 480, 72
Tunnicliffe R. L., Levan A., 2012, in Roming P. W. A., Kawai N., Pian E., eds, Proc. IAU Symp. 279, Death of Massive Stars: Supernovae and Gamma-Ray Bursts. Cambridge Univ. Press, Cambridge, p. 415
Usov V. V., 1992, Nature, 357, 472
Virgili F. J. et al., 2013, ApJ, 778, 54
Xue R. R., Tam P. H., Wagner S. J., Behera B., Fan Y. Z., Wei D. M., 2009, ApJ, 703, 60
Yonetoku D., Murakami T., Nakamura T., Yamazaki R., Inoue A. K., Ioka K., 2004, ApJ, 609, 935
Zaninoni E., 2013, PhD thesis, Università degli Studi di Padova, available at: http://paduaresearch.cab.unipd.it/5626/
Zhang B., Zhang B.-B., Liang E.-W., Gehrels N., Burrows D. N., Mészáros P., 2007, ApJ, 655, L25
Zhang Z. B., Chen D. Y., Huang Y. F., 2012, ApJ, 755, 55
Zhang B.-B., Zhang B., Murase K., Connaughton V., Briggs M. S., 2014, ApJ, 787, 66

APPENDIX A: D'AGOSTINI'S METHOD

For the fit of the correlation that depends on three parameters, $E_{\rm X,iso}$, $E_{\gamma,\rm iso}$, and $E_{\rm pk}$, we use the method of D'Agostini (2005, see equation 70 therein):

$$f(p) = 0.5 \sum \log \Big[p[4]^2 + \sigma(E_{\rm pk})^2 + (p[1]\sigma(E_{\gamma,\rm iso}))^2 + (p[2]\sigma(E_{\rm X,iso}))^2 \Big] + 0.5 \sum \frac{(E_{\rm pk} - p[1]E_{\gamma,\rm iso} - p[2]E_{\rm X,iso} - p[3])^2}{p[4]^2 + \sigma(E_{\rm pk})^2 + (p[1]\sigma(E_{\gamma,\rm iso}))^2 + (p[2]\sigma(E_{\rm X,iso}))^2},$$

with $p[1]$, $p[2]$, and $p[3]$ the coefficients of the function and $p[4]$ the extra-scatter parameter.

Table A1. List of 33 GRBs added to the old sample. Short GRBs are marked in boldface, while the GRB with uncertain classification is underlined.

GRB	z	$E_{\rm X,iso}$ (10^{52})	$E_{\gamma,\rm iso}$ (10^{52} erg)	$E_{\rm pk}$ (kev)
080123	0.495	0.0134 ± 0.0002	0.13[a]	149.50
090426	2.609	0.142 ± 0.011	0.541 ± 0.064	320 ± 54
100117A	0.920	0.020 ± 0.001	0.130 ± 0.015	551 ± 135
100625A	0.452	0.0015 ± 0.0002	0.075 ± 0.003	701 ± 114
110106B	0.618	0.007 ± 0.003	0.734 ± 0.073	194 ± 56
110205A	2.220	8.657 ± 0.075	48.317 ± 6.38	757 ± 305
110213A	1.460	2.243 ± 0.042	5.778 ± 0.813	224 ± 74
110503A	1.613	1.198 ± 0.016	20.817 ± 2.082	551 ± 60
110715A	0.820	0.765 ± 0.016	4.361 ± 0.445	220 ± 22
110731A	2.830	4.058 ± 0.064	49.464 ± 4.946	1164 ± 116
110801A	1.858	0.742 ± 0.021	10.897 ± 2.724	400 ± 171
110818A	3.360	0.594 ± 0.021	26.642 ± 2.756	1116 ± 240
111107A	2.893	0.349 ± 0.023	3.757 ± 0.550	420 ± 124
111117A	1.200	0.010 ± 0.001	0.338 ± 0.106	966 ± 322
111209A	0.677	4.430 ± 0.094	5.139 ± 0.620	520 ± 89
111228A	0.716	0.603 ± 0.008	2.750 ± 0.275	58 ± 7
120119A	1.728	1.326 ± 0.030	27.197 ± 3.626	496 ± 50
120326A	1.798	1.435 ± 0.027	3.267 ± 0.327	152 ± 15
120712A	4.174	1.764 ± 0.126	21.199 ± 2.110	641 ± 130
120802A	3.796	0.336 ± 0.0150	12.886 ± 2.761	274 ± 93
120811C	2.671	2.192 ± 0.061	6.405 ± 0.640	198 ± 20
121128A	2.200	2.489 ± 0.066	8.659 ± 0.866	243 ± 24
130408A	3.758	1.276 ± 0.126	34.972 ± 6.442	1000 ± 140
130427A	0.340	3.480 ± 0.0220	91.891 ± 13.127	1250 ± 150
130505A	2.270	11.848 ± 0.112	346.586 ± 34.659	2030 ± 203
130603B	0.356	0.0129 ± 0.0005	0.212 ± 0.023	966 ± 322
130701A	1.155	0.332 ± 0.008	0.415 ± 0.041	2.283 ± 0.020
130831A	0.479	0.075 ± 0.003	0.126 ± 0.023	1.908 ± 0.032
130907A	1.238	7.921 ± 2.480	2.465 ± 0.027	2.944 ± 0.013
130925A	0.347	2.067 ± 0.042	1.266 ± 0.020	2.387 ± 0.023
131030A	1.295	1.150 ± 0.020	1.482 ± 0.026	2.609 ± 0.023
140206A	2.730	6.560 ± 0.078	1.734 ± 0.079	2.651 ± 0.035
140419A	3.956	7.896 ± 0.092	2.180 ± 0.171	3.160 ± 0.109

[a]Lower limit (D'Avanzo et al. 2014).

This paper has been typeset from a TEX/LATEX file prepared by the author.